IEEE Access
Multidisciplinary | Rapid Review | Open Access Journal

Received November 5, 2021, accepted November 20, 2021, date of publication November 23, 2021,
date of current version December 7, 2021.

Digital Object Identifier 10.1109/ACCESS.2021.3130333

Damping Low-Frequency Oscillations in Power Systems Using Grid-Forming Converters

JOSÉ LUIS RODRÍGUEZ-AMENEDO, (Senior Member, IEEE), AND SANTIAGO ARNALTES GÓMEZ
Electrical Engineering Department, University Carlos III, 28911 Leganés, Madrid, Spain
Corresponding author: José Luis Rodríguez-Amenedo (amenedo@ing.uc3m.es)

This work was supported by the Spanish Research Agency under Project PID2019-106028RB-I00/ AEI/10.13039/501100011033.

ABSTRACT The increasing incorporation of renewable energy in power systems is causing growing concern about system stability. Renewable energy sources are connected to the grid through power electronic converters, reducing system inertia as they displace synchronous generators. New grid-forming converters can emulate the behavior of synchronous generators in terms of inertia provision and other grid services, like power-frequency and voltage-reactive regulation. Nevertheless, as a consequence of synchronous generator emulation, grid-forming converters also present angle oscillations following a grid disturbance. This paper proposes two novel power stabilizers for damping low-frequency oscillations (LFOs) in the power system. The first power stabilizer provides power oscillation damping through active power (POD-P), and it is implemented in a grid-forming converter, using the active power synchronization loop to damp system oscillations by acting on the converter angle. The second one provides power oscillation damping through reactive power (POD-Q), and it is implemented in a STATCOM, using the voltage control loop to damp system oscillations. Both proposals are first assessed in a small-signal stability study and then in a comprehensive simulation. Moreover, two cases are considered: damping the oscillations of a single machine connected to an infinite bus through a tie-line, and damping the inter-area oscillations in a two-area system. Simulation results, as well as the stability study, demonstrate the ability of both stabilizers to damp power system oscillations, being the POD-P more effective than the POD-Q, but at the cost of requiring some kind of energy provision at the DC bus.

INDEX TERMS Grid-forming power converter, STATCOM, power oscillation damping.

I. INTRODUCTION

Power system stability is considered, even today, a key topic in the development and study of modern power systems. As a consequence of increased incorporation of power electronic converter (PEC) interfaced technologies, due mainly to renewable-based energy systems (RESs) and energy storage systems (ESSs), power system dynamic behavior has been significantly altered [1]. The progressive integration of PECs affects rotor angle stability [2] because the system's total inertia is reduced as a consequence of conventional synchronous generator (SG) displacement. This has, in turn, an impact on the system's electromechanical modes (typically in the range of 0.2 Hz to 2 Hz) [3], changing power flows on some tie-lines and affecting the damping of inter-area modes and transient stability margins [4], [5]. Regarding transient stability, lowering the system's total inertia may result in faster and larger rotor swings, making the system more prone to stability problems. However, studies have shown that increased incorporation of PECs can have pros and cons, depending on the grid layout, location and PEC control strategy [6].

In this paper, the stability problem analyzed is related to small-signal stability, which is defined as the ability of the power system to maintain synchronism when subject to small disturbances [7]. In today's practical power system, the small-signal problem is usually one of insufficient damping oscillation due to a lack of SG damping torque. As a consequence, when some groups of closely coupled SGs are connected by weak tie-lines, inter-area oscillation modes occur at low frequency. These oscillations are undesirable as they result in suboptimal power flows and inefficient operation of the grid. Therefore, damping of these power oscillations is of vital concern.

The associate editor coordinating the review of this manuscript and approving it for publication was Wencong Su.

Traditionally, power system stabilizers (PSSs), implemented on SGs, have been used to damp these low-frequency oscillations. The basic function of a PSS is therefore to add damping to the generator rotor oscillations by controlling excitation using an auxiliary stabilizing signal. To provide damping, the stabilizer must produce a component of electrical torque in phase with the rotor speed deviations. A PSS typically consists of three blocks [7]: a gain block, a washout block to cancel any DC component of the input signal, and a phase compensation block to compensate the phase lag between the exciter input and the electrical torque. There are several PSS types: the delta-omega PSS is a stabilizer based on shaft speed signal, the delta-P-omega PSS estimates the rotor speed deviation from a signal proportional to the integral of the electrical power change. Other stabilizers use the terminal frequency as the stabilizing signal. The sensitivity of the frequency signal to rotor oscillation increases as the external transmission systems become weaker. One of the major limitations of PSS design is parameter tuning. Even in the simplest models the following parameters must be adjusted: PSS gain, washout filter time constant and lead-lag time constants of the phase compensator [8]. These parameters are tuned once, usually during the commissioning of the generator, and remain constant independently of operating conditions [9].

To overcome the inter-area oscillation wide-area based PSSs have been recently proposed with remote signals obtained from PMU devices [10]. Also, new devices based on PECs are proposed. Flexible AC Transmission Systems (FACTS), both in shunt and series configurations, have been widely used to enhance power system stability [11]. In the specific case of shunt-connected FACTS, Static Var Compensators (SVCs) and STATCOMs, power oscillation damping (POD) can be achieved by modulating the voltage at the point of common coupling (PCC) using reactive power injection. However, this solution has a drawback since the voltage in the PCC must be regulated within specified limits (usually $\pm 10\%$ of the rated voltage), which reduces the damping that this device can provide. Moreover, the amount of injected reactive power needed to modify the voltage at the PCC depends on the short-circuit ratio (SCR). The higher the SCR, the more reactive power is needed to change the voltage at the PCC. Since this type of device uses reactive power to damp power oscillations, the acronym POD-Q will be used throughout this paper. On the other hand, injection of active power (on reactive transmission lines) affects the PCC voltage-angle without varying the voltage magnitude significantly. When active power is used as a stabilizer, the controller is named a POD-P. In [12], the control strategy of an E-STATCOM (STATCOM with energy storage) is presented to optimize the injection of active and reactive power to provide uniform damping at different locations in the power system. In [13], the same E-STATCOM concept is used to mitigate forced oscillations. Resonant controllers are adopted to perform closed-loop control of active and reactive power. In both cases, a phase-locked loop (PLL) is used to implement the control proposed. POD-P has also been implemented on VSC-HVDC systems connected to offshore wind farms [14], where practical implementation issues such as robustness against control/communication delays, and limitation of PODs due to mechanical resonances on wind turbine generators, are considered. In [15], fundamental performance limitations in utilizing HVDC to damp inter-area modes are investigated.

Damping LFOs in power system using energy storage systems (ESS) and renewable power plants has been recently published. In [16] a heuristic dynamic programming method is used to control ESS to damp inter-area oscillations. Likewise, in [17] subsynchronous oscillation damping is investigated through full-converter wind turbines and in [18] through PV plants.

One step ahead in improving grid stability are grid-forming converters (GFCs), a well-known solution that can provide a fast response in the event of disturbance in the power system [19]. GFCs use a synchronization loop to emulate an SG through a droop constant [20], or as a virtual synchronous machine (VSM) [21], including the inertia constant in the control. These two approaches have been developed in two separate contexts, but they can be equivalent as shown in [22]. In any case, the main difference between GFCs and other types of converters, such as grid-following converters (GFLs), is that GFCs can be represented as a voltage source behind an impedance without using a PLL to follow the grid voltage angle. Different GFC strategies have been proposed recently, among which it is worth mentioning the synchronverter [23], which emulates SGs without using any specific synchronization unit, or the synchronous power converter (SPC) [24], whose operating principle is based on determining the internal frequency deviation from a second-order function applied to the variation between the measured and reference active powers. This method uses an additional frequency loop to modify the active power reference when a deviation exists between the reference frequency and the frequency recorded by a PLL. Droop control and VSG control are merged into a generalized droop control [25] which meet the demand for different dynamic characteristics in grid-connected and stand-alone modes at the same time.

In [26], a grid-forming converter tuning method for damping subsynchronous interaction in electrical grids using artificial intelligence is presented. All the aforementioned techniques use an active power synchronization (APS) loop; however, a similar technique based on reactive power synchronization (RPS) has been reported in [27] and [28]. In [29], the POD-P control proposed acts on the internal frequency deviation of the synchronization loop using the active power increment as input. Also, it investigates how a VSM affects the LFOs in power systems by analyzing its equivalent damping torque and the influence of the grid frequency detector from a PLL, which has a negative damping effect on the LFOs. This negative damping effect is reduced by using a phase compensation method.

In this paper, a different proposal is employed for damping low-frequency oscillations. Initially, the frequency deviation at the GFC output terminal is measured and used as the stabilizing signal of a PSS block composed only of a washout filter and a gain, so as to calculate a compensation deviation frequency added to the synchronization loop. In this way, when power oscillation is detected through the deviation frequency measured at the output terminals, the GFC acts and injects active power to damp the oscillation. The time constant of the washout filter guarantees that the PSS is only operative for low-frequency oscillations and cancels any DC component of the input signal. An advantage of this system, compared to the conventional PSS of SGs, is that no phase compensation block is necessary, which significantly simplifies its design and tuning.

This paper is organized as follows: Section II presents the system description and modelling of a SG connected to an infinite bus when a PEC is connected at the generator bus with the proposed POD-P and POD-Q stabilizers. In Section III a small-signal stability analysis and a time-domain simulation comparing LFOs damping modes are presented. In Section IV, a two-area benchmark is described following the specifications of the Spanish regulation on the assessment of the requirements for generators [30]. The system eigenvalues are analyzed using different POD stabilizers and under variation of the interconnection line parameters. Subsequently, the dynamic response of the system is studied for a load change and a line tripping. In Section V, the conclusions of this paper are discussed.

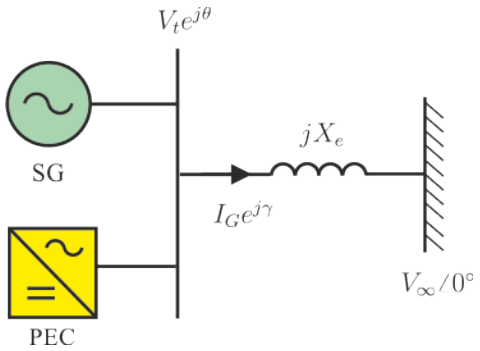

FIGURE 1. Single-machine infinite-bus system with a PEC.

II. SYSTEM DESCRIPTION AND MODELLING

Fig. 1 shows a synchronous generator connected to an infinite bus, through a reactance X_e, where a power electronic converter (PEC) is connected at the generator bus, as indicated in the figure, with the purpose of damping the power oscillations. At the generator bus the voltage vector is represented by $V_t e^{j\theta}$, where V_t is the voltage magnitude and θ its angle with respect to infinite bus $V_\infty \angle 0°$. The current injected into the line is denoted as $I_G e^{j\gamma}$.

A reduced-order SG model [31], [32] is typically employed for low-frequency oscillations studies. In this article, a one-axis (flux-decay) model is used that does not consider the stator/network and the faster damper-winding dynamics, having only the state variable E'_q, which is proportional to the field flux and oriented to the quadrature axis, q. The other three state variables are a) angle δ between the q-axis of the SG with respect to the reference voltage $V_\infty \angle 0°$; b) generator speed ω; and c) excitation voltage E_{fd}. Linearizing the dynamic equations on a given operating point results in a new state-space model that it is used to examine the eigenvalues, as well as to design supplementary controllers to ensure adequate damping of dominant modes.

The dynamic equations of the SG [34] are given following:

$$T'_{d0}\frac{dE'_q}{dt} = -E'_q - \left(X_d - X'_d\right) I_d + E_{fd} \tag{1}$$

$$2H\frac{d\omega}{dt} = T_m - T_e - D(\omega - 1) \tag{2}$$

$$\frac{1}{\omega_s}\frac{d\delta}{dt} = \omega - 1 \tag{3}$$

$$T_A\frac{dE_{fd}}{dt} = -E_{fd} + K_A\left(V_{ref} - V_t\right) \tag{4}$$

where T'_{d0} is the d-axis open-circuit transient time constant, with X_d and X'_d being the total and transient d-axis reactance, respectively. H is the inertia constant of the generator, expressed in seconds, D is the damping constant, and ω is the angular velocity of the rotor, in p.u. The dynamic equation of δ (3) is obtained by integrating the rotational speed of the generator, ω, with respect to a synchronously rotating reference, ω_s, in rad/s. The dynamic equation of E_{fd} (4) has been obtained assuming a fast exciter for regulating voltage V_t at the output bus from a reference voltage V_{ref}. In (4) T_A and K_A are the time constant and the gain of the exciter, respectively.

To complete the set of equations that define the dynamic behavior of the generator, the following algebraic equations of the stator and network must be added. The stator algebraic equations, according [33], are

$$X_q I_q - V_d = 0 \tag{5}$$

$$E'_q - V_q - X'_d I_d = 0 \tag{6}$$

Fig. 2 shows the equivalent circuit of the single-machine infinite-bus system with a PEC. The PEC is represented by an independent voltage source $E_g e^{j\delta_g}$ behind a reactance X_g.

The SG is modelled as a dependent voltage source $\overline{E}_{SG}$

$$\overline{E}_{SG} = \left[\left(X_q - X'_d\right) I_q + jE'_q\right] e^{j\left(\delta - \frac{\pi}{2}\right)} \tag{7}$$

behind reactance X'_d.

The algebraic network equations are obtained by calculating $V_t e^{j\theta}$, in Fig. 2, in terms of the independent voltage source $E_g e^{j\delta_g}$ and the reference voltage $V_\infty \angle 0°$.

Applying Millman's theorem to the equivalent circuit of Fig. 2 obtains the following:

$$\begin{aligned} V_t e^{j\theta} &= \left(V_d + jV_q\right) e^{j\left(\delta - \frac{\pi}{2}\right)} \\ &= +K'_d\left[\left(X_q - X'_d\right) I_q + jE'_q\right] e^{j\left(\delta - \frac{\pi}{2}\right)} \\ &\quad + K_g jE_g e^{j\left(\delta_g - \frac{\pi}{2}\right)} + K_e V_\infty \end{aligned} \tag{8}$$

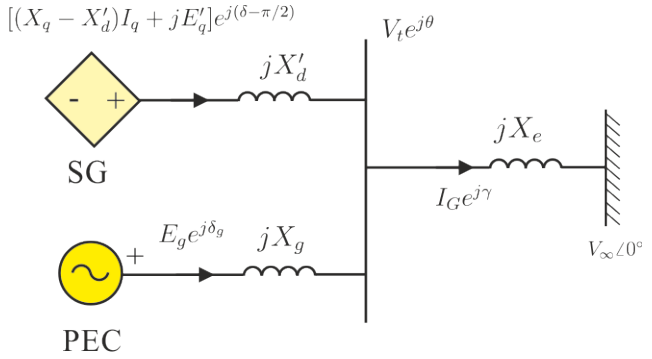

FIGURE 2. Synchronous machine one-axis equivalent circuit with a PEC.

where K'_d, K_g and K_e are expressed as

$$K'_d = \left(\frac{\overline{Y}'_d}{\overline{Y}'_d + \overline{Y}_g + \overline{Y}_e}\right) = \frac{X_g X_e}{X_g X_e + X'_d X_e + X'_d X_g} \quad (9)$$

$$K_g = \left(\frac{\overline{Y}_g}{\overline{Y}'_d + \overline{Y}_g + \overline{Y}_e}\right) = \frac{X'_d X_e}{X_g X_e + X'_d X_e + X'_d X_g} \quad (10)$$

$$K_e = \left(\frac{\overline{Y}_e}{\overline{Y}'_d + \overline{Y}_g + \overline{Y}_e}\right) = \frac{X'_d X_g}{X_g X_e + X'_d X_e + X'_d X_g} \quad (11)$$

being the admittances $\overline{Y}'_d = -j/X'_d$, $\overline{Y}_g = -j/X_g$ and $\overline{Y}_e = -j/X_e$. As these admittances have only imaginary part K'_d, K_g and K_e appear as constants in (8).

By multiplying (8) by $e^{-j(\delta-\frac{\pi}{2})}$ and separating the real and imaginary parts, the following algebraic equations of the network are obtained:

$$V_d - K'_d\left(X_q - X'_d\right) I_q + K_g E_g \sin\left(\delta_g - \delta\right) - K_e V_\infty sin\delta = 0 \quad (12)$$

$$V_q - K'_d E'_q - K_g E_g \cos\left(\delta_g - \delta\right) - K_e V_\infty cos\delta = 0 \quad (13)$$

The active and reactive power injected by the PEC into the grid are expressed as

$$P_g = \left(\frac{V_t}{X_g}\right) E_g \sin\left(\delta_g - \theta\right) \quad (14)$$

$$Q_g = \left(\frac{V_t}{X_g}\right)\left[E_g \cos\left(\delta_g - \theta\right) - V_t\right] \quad (15)$$

The power converter is controlled by acting on the voltage magnitude E_g or on the angle δ_g. As is well known, voltage control mainly affects reactive power Q_g, while, angle control determines active power P_g.

PEC control will be designed to damp transmitted power oscillations through the line by acting on the exchanged active and reactive power. This paper proposes a novel PSS for grid-forming converters and compares it to the PSS implemented in a STATCOM. In the first case, power oscillation damping is achieved by exchanging active power; while the STATCOM uses only reactive power. The fundamentals of these stabilizers are presented below.

A. GRID FORMING CONVERTER STABILIZER

A grid-forming converter differs from a GFL mainly in that a GFC behaves as a voltage source with a low series impedance, while a GFL can be approximated to a controlled current source with a high parallel impedance. Furthermore, a GFC uses a power synchronization loop without a PLL.

As illustrated in Fig. 3, the synchronization loop sets the power angle δ_g, which determines the q-axis position of internal voltage source $E_g e^{j\delta_g}$ with respect to reference voltage $V_\infty \angle 0°$, based on the difference between power reference P^*_g and actual power P_g. As stated in (14), the active power of the GFC depends on δ_g and the voltage at the output terminals $V_t e^{j\theta}$. The rotational speed of the dq-axes on the GFC is denoted as the difference between ω_g and reference frequency ω_s.

Considering that ω_g is expressed in p.u., power angle δ_g is calculated as

$$\frac{1}{\omega_s}\frac{d\delta_g}{dt} = \omega_g - 1 \quad (16)$$

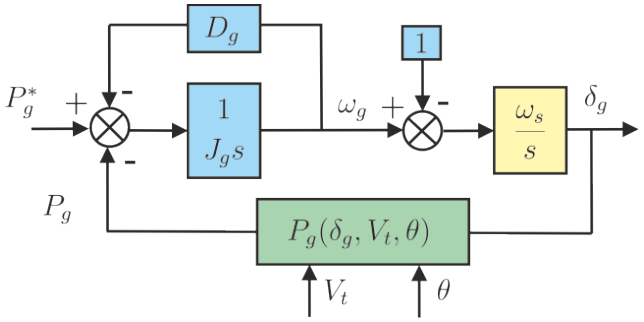

FIGURE 3. Grid-forming converter power synchronization loop.

Note that this equation is completely analogous to that indicated in (3) corresponding to a synchronous generator.

According to Fig. 3, frequency ω_g is obtained as

$$\omega_g = \frac{P^*_g - P_g}{J_g s + D_g} \quad (17)$$

where J_g is the inertia constant of the GFC (in seconds), D_g is the damping constant, and its inverse $R_g = 1/D_g$ is the droop constant that, in p.u., is the ratio of normalized frequency variation $\Delta f/f_n$ and normalized power deviation $\Delta P/P_n$. If the inertia constant is equal to zero, ω_g is calculated as the product of a droop constant and the active power increment with respect to a reference, $\omega_g = R_g(P^*_g - P_g)$.

Power oscillation damping using a GFC is carried out by acting on the power synchronization loop as shown in Fig. 4. By measuring the frequency at the output terminals of the GFC, ω, frequency ω' in the synchronization loop is determined using a washout function of the form

$$\omega' = K_w\left(\frac{T_w s}{T_w s + 1}\right)\omega \quad (18)$$

This function is similar to that of a conventional PSS of an SG without considering the phase compensation block that

is used regarding the dynamic between the generator exciter and the generator torque.

The frequency range that is usually compensated is between 0.1 Hz and 2 Hz. The washout function acts as a high-pass filter with a sufficiently high time constant T_w (0.1 to 20 s) to ensure that the low-frequency oscillations measured in the bus are not altered

Furthermore, the washout filter blocks any DC component that could appear in the bus due to a permanent frequency deviation with respect to ω_s. In this way, the PSS works only when there are slow frequency variations, and K_w is tuned to ensure that the oscillation modes have sufficient damping.

The proposed PSS acts directly on angle δ_g, since a pole-zero cancellation occurs between the compensation block and the integral function ω_s/s, which implies a direct variation of active power P_g. A PSS like this could also be implemented in a GFL converter by calculating the active power reference as a function of the frequency measured in the bus. However, its effectiveness is not as immediate as in the case of the GFC due to the dynamics between P_g^* and P_g. There is a variant to this PSS used in GFCs, which is based on calculating the active power reference using the internal frequency variation of the synchronization loop through the washout function indicated in (18). Fig. 5 shows the implementation of this option. The advantage of this method is that direct measurement of the frequency in the bus is not required, although it can give rise to some stability problems [34].

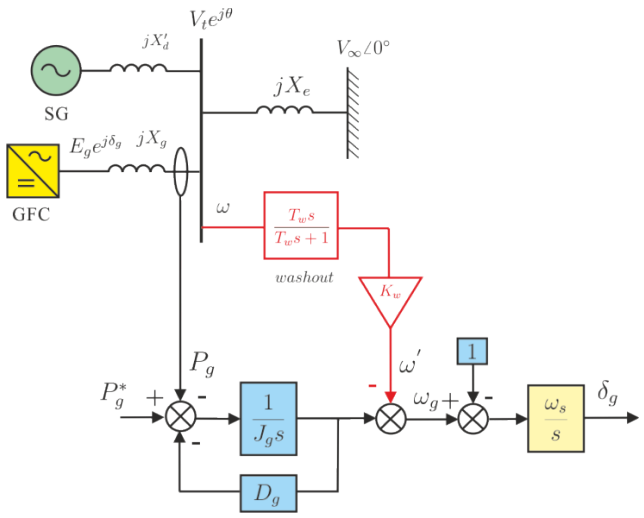

FIGURE 4. Power oscillation damping block diagram in a GFC.

As described above, the proposed control system acts on angle δ_g, keeping voltage magnitude E_g constant. Furthermore, if E_g matches V_t, reactive power Q_g is approximately zero. The corresponding linearized GFC model has been considered with $J_g = 0$ and the PSS based on the frequency measurement.

Frequency deviation $\Delta\omega_g$ is equal to

$$\Delta\omega_g = -R_g \Delta P_g = -R_g K_s \left(\Delta\delta_g - \Delta\theta\right) \tag{19}$$

where ΔP_g is obtained by linearizing (14) when E_g is kept constant, being the synchronization constant K_s

$$K_s = \left(\frac{V_t^0 E_g^0}{X_g}\right) \cos\left(\delta_g^0 - \theta^0\right) \tag{20}$$

Considering that $X_g = 0.15$ p.u., $V_t^0 = E_g^0 = 1$ p.u., and $\delta_g^0 = \theta^0$, the synchronization constant value is $K_s = 6.67$ p.u. This value is significantly higher than that of a conventional SG, according to the parameter values given in Table 1 (Annex A). This means that active power transmission is produced with lower power angles.

The PSS transfer function of (18) is represented in the block diagram of Fig. 6. The deviation of frequency compensation $\Delta\omega'$, according to Fig. 6, is expressed in terms of the frequency deviation in the bus, $\Delta\omega$, and an auxiliary state variable, Δz, as

$$\Delta\omega' = K_w \left(\Delta\omega - \Delta z\right) \tag{21}$$

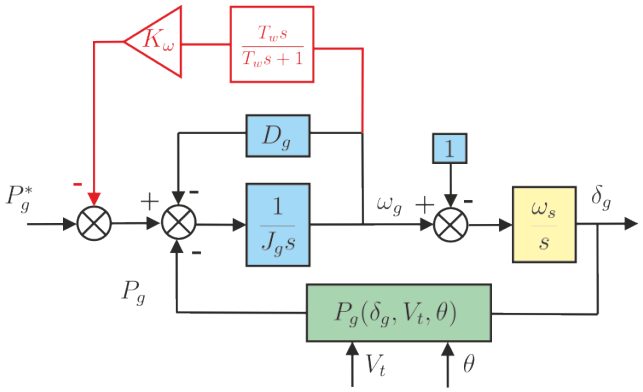

FIGURE 5. Grid-forming converter with an internal PSS.

Fig. 7 shows the linearized block diagram of the GFC with power oscillation damping based on active power (POD-P).

The active power reference increment is considered null, $\Delta P_g^* = 0$, and ΔP_g is obtained, according to (19), as the difference of angles $\Delta\delta_g$ and $\Delta\theta$.

The increment of the angle in the bus, $\Delta\theta$, can be expressed in terms of the state variable $\Delta\delta$ and the algebraic variables ΔV_d and ΔV_q linearizing $V_d = V_t \sin(\delta - \theta)$ as

$$\Delta\theta = \Delta\delta + \left(\frac{E_g^0}{X_g K_s}\right)\left[\Delta V_t sin\left(\delta^0 - \theta^0\right) - \Delta V_d\right] \tag{22}$$

where ΔV_t is expressed as a function of ΔV_d and ΔV_q according to

$$\Delta V_t = \left(\frac{V_d^0}{V_t^0}\right)\Delta V_d + \left(\frac{V_q^0}{V_t^0}\right)\Delta V_q \tag{23}$$

With the connection of the GFC to the SG bus, the set of dynamic equations of the system is increased by two. Linearizing (16) and considering the increment of frequency

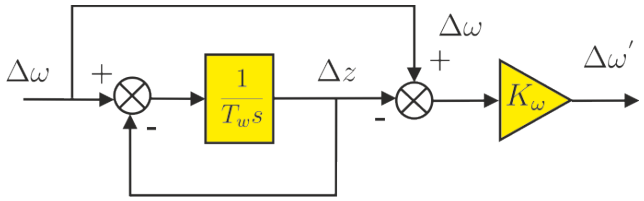

FIGURE 6. PSS block diagram.

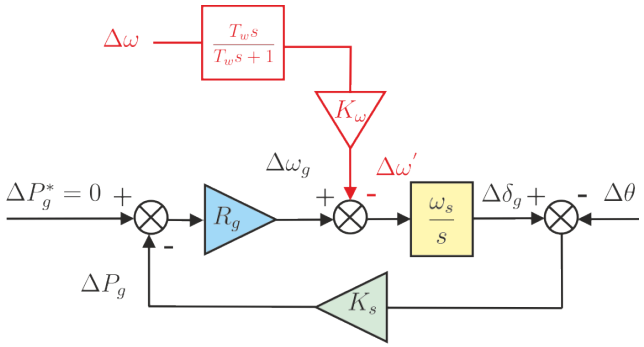

FIGURE 7. Linearized block diagram of a GFC with a POD-P.

$\Delta\omega'$ in the synchronization loop, the dynamic equation of $\Delta\delta_g$ is obtained as

$$\frac{1}{\omega_s}\frac{d\Delta\delta_g}{dt} = -R_g K_s\left(\Delta\delta_g - \Delta\theta\right) - K_w\left(\Delta\omega - \Delta z\right) \quad (24)$$

Likewise, the dynamic equation of the auxiliary variable Δz of the PSS (Fig. 6) is equal to

$$T_w\frac{d\Delta z}{dt} = \Delta\omega - \Delta z \quad (25)$$

These two last equations, together with those corresponding to the dynamics of the generator (1)-(4), complete the set of dynamic equations of the system, which is now of the 6th order. The number of algebraic equations remains four, the first two (5)–(6) correspond to the SG and the other two are obtained by linearizing (12) and (13) assuming that E_g is constant. Using this set of differential-algebraic equations, matrices A, B, C and D of the linearized model are obtained. The analytical expression of these matrices is indicated in Appendix B.

B. STATCOM STABILIZER

In the case of a STATCOM, power oscillation damping is carried out through voltage control similarly to the conventional PSS of an SG, but without using a phase compensator. As it is well-known, the PSS of a SG acts on the excitation system of the generator, hence affecting its terminal voltage which in turn affects the generator power a per equation (14) for damping the generator rotor angle swings. Thus, the STATCOM can stabilize the rotor swings in the same way, by modifying the bus voltage through the injection of reactive power.

For transient stability studies, a STATCOM model is represented by a set of algebraic equations and a unique state variable corresponding to the DC link voltage [35]. However, in order to simplify the analysis, it has been considered that the STATCOM only exchanges reactive power in such a way that $\delta_g = \theta$. Note that, according to (14), P_g depends on $sin\left(\delta_g - \theta\right)$ such that $P_g = 0$ when both angles are equal.

Now, power oscillation damping is carried out by adding to reference voltage E_g^* the output of washout function E_g', as shown in Fig. 8.

According to (15), and assuming that $\delta_g = \theta$, the reactive power exchange by the STATCOM only depends on voltage E_g with respect to bus voltage V_t.

$$Q_g = \frac{V_t}{X_g}\left(E_g - V_t\right) \quad (26)$$

The power oscillation damping implemented in this case is calculated by modifying reference voltage E_g^* with compensation voltage E_g', which is obtained from the frequency measured in the bus using the same washout function as in the previous case.

$$E_g' = K_w\left(\frac{T_w s}{T_w s + 1}\right)\omega \quad (27)$$

but with the difference that the output signal is a voltage instead of a frequency. As the voltage variation gives rise to a reactive power exchange, the compensator is denoted as POD-Q.

Linearizing (27), ΔE_g is now different to zero and equal to

$$\Delta E_g = K_w\left(\Delta\omega - \Delta z\right) \quad (28)$$

which depends on variable states.

The only additional differential equation with respect to the single-machine infinite-bus model is the one corresponding to the washout function, and its expression is the same as (25). In this case, the set of dynamic equations of the system is of the 5th order and the algebraic equations are the same as in the previous case. However, matrices A, B, C and D are different since now $\Delta E_g'$ is not null and depends on the state variables $\Delta\omega$ and Δz. The expression of the matrices of the linearized model is also given in Appendix B.

III. STABILITY ANALYSIS

A. SMALL-SIGNAL STABILITY

In this section, the small-signal stability is analyzed. The model parameters used in the analysis are given in Table 3 of Annex A. The eigenvalues of the linearized system with and without PEC stabilizer are obtained and the corresponding oscillation modes analyzed.

To obtain the system state matrix, the parameters of Table 3 are required as well as the state values and the algebraic variables at the operation point. These values are obtained by defining the voltage magnitude, and its angle, at the generator bus with respect to the infinite bus $V_\infty = 1p.u.$ In this case, when $V_t = 1$ p.u. and $\theta = 9^0$, the corresponding state values and algebraic variables are those indicated in Table 4 of Annex A.

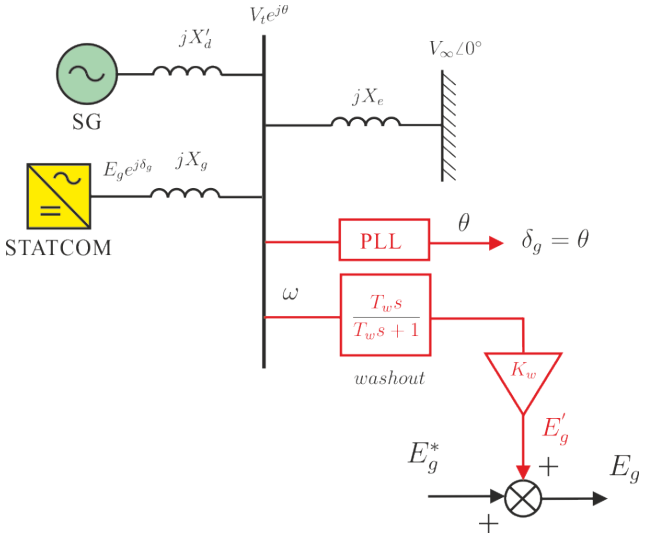

FIGURE 8. STATCOM power oscillation damping block diagram.

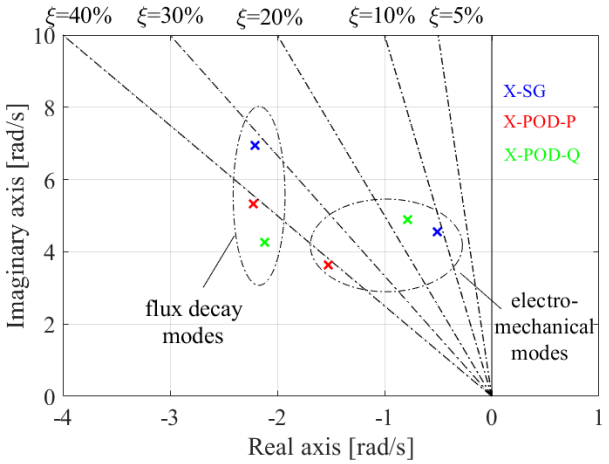

FIGURE 9. Eigenvalue loci for a single-machine infinite-bus system (SG in blue), with a GFC (POD-P in red), and with a STATCOM (POD-Q in green).

Fig. 9 shows the electromechanical and the flux-decay modes of the single-machine infinite-bus case in blue. The oscillation modes of the system are shown in red when the GFC with the POD-P is connected to the generator bus. Likewise, the eigenvalues for the STATCOM with a POD-Q case are represented in green.

Comparing the POD-P with the baseline case (SG without a PEC connected) reveals that the electromechanical oscillation mode is significantly damped up to a damping factor of 40.2%. Nevertheless, the natural frequency is only slightly lower, 0.58 Hz. In the STATCOM case, oscillation damping is not as effective when compared to the electromechanical oscillation mode, which is only damped up to 15.84%. Furthermore, the natural oscillation frequency is quite similar to the baseline case, 0.78 Hz. By acting directly on the voltage, the POD-Q control has a direct action on the flux-decay, its damping factor being significantly higher, 44.47%.

Table 1 shows, for the three cases analyzed, the system eigenvalues and the corresponding damping factor and natural frequency, as well as the participation factors for each state variable.

For the baseline case, the electromechanical mode λ_{12} is dominated by the states $\Delta\omega$ and $\Delta\delta$, its participation factors being 0.38 for each state. Regarding the flux-decay mode λ_{34}, its dominant states are $\Delta E'_q$ and ΔE_{fd} with a participation factor of 0.41 and 0.39, respectively. When this same analysis is carried out for the GFC, the participation factors are more distributed between the states $\Delta E'_q$, $\Delta\omega$, $\Delta\delta$ and ΔE_{fd} for the electromechanical and flux-decay modes. In the GFC case, two additional non-oscillatory stable eigenvalues, λ_5 and λ_6, are observed. The eigenvalue λ_5 is completely dominated by the state $\Delta\delta_g$, with a participation factor of 0.95 and a natural frequency of 6.74 Hz that is higher than those registered in the baseline case. Likewise, the eigenvalue λ_6 is dominated by the auxiliary state Δz, corresponding to the washout filter with a participation factor of 0.96 and a natural frequency of 0.16 Hz. These two eigenvalues have not been represented in Fig. 9. In the STATCOM case, the electromechanical mode is slightly modified, the participation factors of this mode being very similar to the baseline case. For the flux-decay mode, a greater contribution of state $\Delta\delta$ and a lower contribution of states $\Delta E'_q$ and ΔE_{fd} are observed. The non-oscillatory mode λ_5, corresponding to the washout filter, presents a similar natural frequency to the previous case, 0.15 Hz, and is not represented in Fig. 9 either.

B. EIGENVALUE LOCI UNDER VARIATION OF POWER STABILIZER PARAMETERS

This section shows the loci of the eigenvalues corresponding to the electromechanical and flux decay modes under variation of parameters K_W and T_W of the power stabilizer. It has been considered that the stabilizer gain K_W varies from 0 to 5 p.u for three time constant, T_W, values, 0.1, 0.5 and 1.0 s.

TABLE 1. Eigenvalues, damping factor and natural frequency, as well as the participation factors for the three cases analyzed.

EIGENVALUES	ξ (%)	ω_n (Hz)	$\Delta E'_q$	$\Delta\delta$	$\Delta\omega$	ΔE_{fd}	$\Delta\delta_g$	Δz
SG (baseline case)								
$\lambda_{12} = -0.51 \pm j4.55$	11.17	0.72	0.14	0.38	0.38	0.10	0.00	0.00
$\lambda_{34} = -2.21 \pm j6.95$	30.25	1.10	0.41	0.10	0.10	0.39	0.00	0.00
GFC (POD-P)								
$\lambda_{12} = -1.52 \pm j3.63$	40.20	0.58	0.32	0.25	0.17	0.10	0.01	0.02
$\lambda_{34} = -2.22 \pm j5.33$	40.30	0.85	0.24	0.27	0.24	0.20	0.03	0.02
$\lambda_5 = -42.38$	100	6.74	0.00	0.00	0.05	0.00	0.95	0.00
$\lambda_5 = -1.03$	100	0.16	0.00	0.04	0.00	0.00	0.00	0.96
STATCOM (POD-Q)								
$\lambda_{12} = -0.78 \pm j4.90$	15.84	0.78	0.19	0.37	0.31	0.12	0.00	0.01
$\lambda_{34} = -2.12 \pm j4.27$	44.47	0.68	0.39	0.17	0.10	0.32	0.00	0.02
$\lambda_5 = -0.95$	100	0.15	0.00	0.04	0.00	0.00	0.00	0.96

Fig. 10 shows the eigenvalues loci for the single-machine infinite-bus case when a GFC is connected at the SG bus and a POD-P is employed. Electromechanical modes are shown in

the upper-right of the figure. As can be seen, the eigenvalues start from the same point regardless of T_W when $K_W = 0$. For a low time, constant value ($T_W = 0.1$ s) the damping remains practically constant and the oscillation frequency is slightly reduced. On the contrary, for high time constant values ($T_W =$ 0.5 s and 1.0 s) the damping increases when K_W increases and the oscillation frequency remains constant.

For the flux decay modes when K_W increases, the damping increases for low time constant. For high time constants ($T_W = 0.5$ s and 1.0 s) the eigenvalues move from left to right decreasing the damping. As it can be seen in Fig. 10, for $T_W = 0.5$ s and 1.0 s, the evolution of the damping is the opposite for electromechanical and flux decay modes when K_W increases. For this reason, once the time constant of the stabilizer is selected, increasing the gain K_W for damping electromechanical modes is limited to avoid poor damping of flux decay modes.

In addition, a high stabilizer gain also increases the active power exchanged, which also limits the maximum value of K_W, because a PEC with a higher rating is required.

Fig. 11 shows the eigenvalue loci for a single-machine infinite-bus when a STATCOM is connected at the SG bus and a POD-Q is employed. In this case the damping of electromechanical modes is quite limited. Moreover, for a low value of T_W, the damping is reduced when K_W increases. Only for high values of T_W a moderated damping increase is obtained, but it decreases if K_W is too high.

For the electromechanical modes the oscillation frequency decreases when K_W increases. While, for the flux decay modes, the evolution of the eigenvalues is just in the opposite direction, the oscillation frequency increases when K_W increases and the damping remains practically constant.

As conclusion, it can be said that the GFC (POD-P) is quite effective for damping electromechanical modes, but limiting the value of the stabilizer K_W gain, since high values can give rise to poorly damped modes of flux decay. Regarding the STATCOM (POD-Q), the flux decay modes are always well damped, but it is not as effective for damping the electromechanical modes.

C. TIME-DOMINE RESPONSE

This section provides the response of the active and reactive power transmitted through the line to a torque step of 0.5 p.u. in the generator at t = 0 for the three cases analyzed. Fig. 12 shows the active power response.

As can be seen in Fig. 12, the POD-Q slightly damps the response of the active power transmitted through the line compared to the baseline case, reaching the steady state without oscillations in about 10 s. In contrast, the POD-P damps the power oscillation in just 3 s, presenting only two oscillations before reaching steady state. The first oscillation is negative, with a peak value of −0.2 p.u. A similar response for the reactive power is shown in Fig. 13. In this case, no negative response is registered during the first oscillation.

These results are in accordance with the eigenvalue analysis performed in the previous sub-sections.

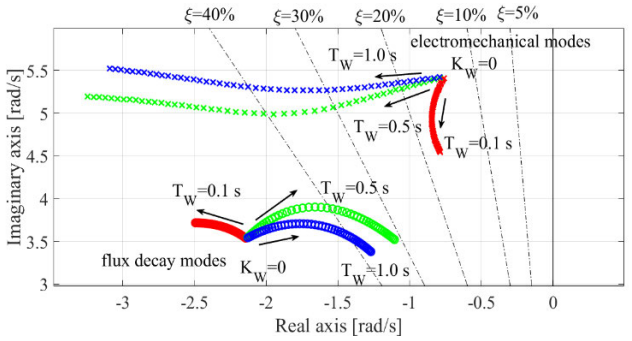

FIGURE 10. Eigenvalue loci for a single-machine infinite-bus system with a SG and a GFC (POD-P) under variations of parameters K_W (from 0 to 5 p.u) and T_W (0.1, 0.5, and 1.0 s).

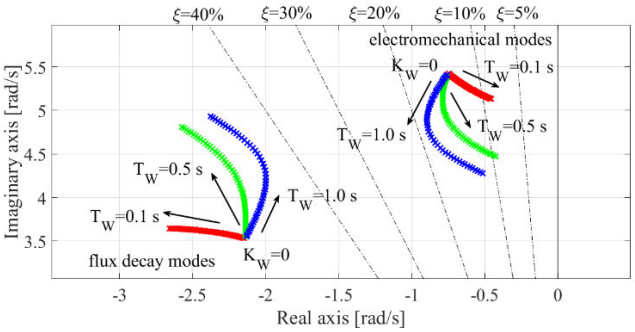

FIGURE 11. Eigenvalue loci for a single-machine infinite-bus system with a SG and a STATCOM (POD-Q) under variations of parameters K_W (from 0 to 5 p.u) and T_W (0.1, 0.5, and 1.0 s).

IV. TWO-AREA SYSTEM

The control schemes proposed in the previous sections will be employed here to study the damping of inter-area oscillations. These oscillations appear when two synchronous areas are connected by a weak tie-line.

Fig. 14 shows the single line diagram of a two-area system following the specifications of the Spanish regulation on assessment of requirements for generators [31].

This system consists of two synchronous generators, SG1 and SG2, connected through their corresponding step-up transformers, and interconnected through two parallel lines between buses 2 and 3. On bus 2, a PEC is also connected through a transformer. The synchronous generator connected at bus 1 has a rating of 1500 MVA. The power rating of the synchronous generator connected at bus 4 is 4000 MVA. In steady state, each line between buses 2 and 3 transmits 50 MW and the active and reactive power injected by the PEC is zero. The PEC power rating is the same as SG1, 1500 MVA, and it does not act until a disturbance arises in the system, following its control scheme. Table 2 shows the steady-state characteristics of generators and loads.

It is considered that reactance X_L corresponding to the tie-line between buses 2 and 3, is variable, with values in the range of 0.01 to 0.9 p.u., the power rating being 100 MVA. Short-circuit reactance of the transformer connected between buses 3 and 4 is equal to 0.003 p.u., and to 0.01 p.u. for the transformers connecting buses 1–2 and 5–2. In all cases,

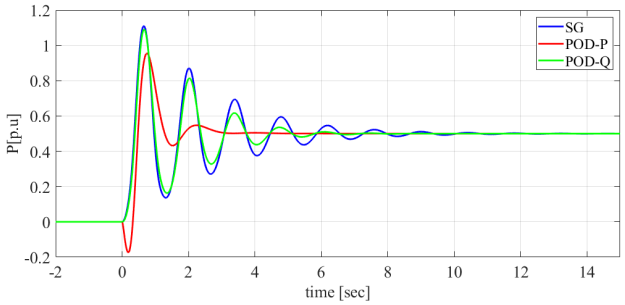

FIGURE 12. Active power response to a torque step of 0.5 p.u. in the generator at t = 0 s for the three cases analyzed: a) SG b) POD-P (GFC) and c) POD-Q (STATCOM).

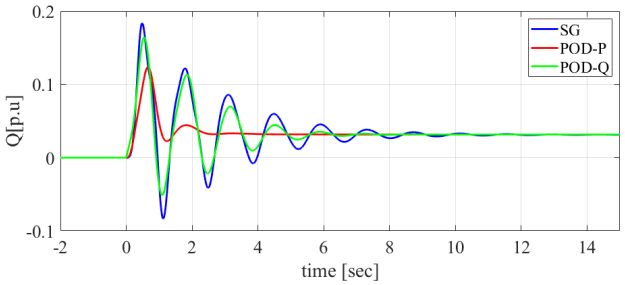

FIGURE 13. Reactive power response to a torque step of 0.5 p.u. in the generator at t = 0 s for the three cases analyzed: a) SG b) POD-P (GFC) and c) POD-Q (STATCOM).

a power base of 100 MVA has been considered. Loads connected in buses 2 and 3 are modeled as ZI loads, assuming constant current for the active power and constant impedance for the reactive power.

The synchronous generators SG1 and SG2 are modeled using a GENROU model [36] for the electrical machine, an IEEE-ST1 excitation model [8], and an IEEEG1 for the steam turbine and speed governor models. All parameters of these models are given in Appendix C.

A. EIGENVALUE LOCI UNDER VARIATION OF PARAMETERS

The oscillation modes of the two-area system shown in Fig. 14 are studied below when reactance X_L of the tie-line between buses 2 and 3 is varied between 0.01 p.u. and 0.9 p.u. The cases to be analyzed are the same as those presented in Section V. First, the low-frequency oscillation modes of the system (electromechanical and flux-decay modes of the generators) are analyzed when the PEC is not connected.

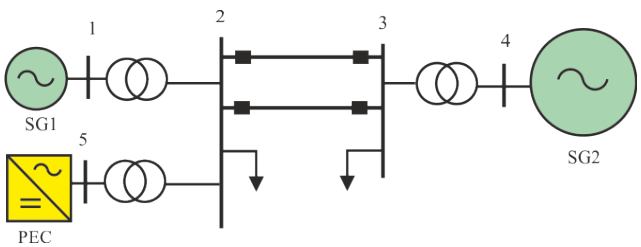

FIGURE 14. Single line diagram of two-area system with a PEC.

Next, oscillation mode analysis is carried out with the PEC connected to bus 2 using a POD-P and a POD-Q control strategy. In this section, a numerical method for computing the eigenvalues of the two-area system is used. This method is extensively used in the bibliography [37]–[39].

Although the stability problem for the two-area system could have been studied analytically, as in Sections III, the numerical method has been preferred in order to avoid making the exposition overly cumbersome. Mainly, small-signal stability analysis can be addressed through time-domain methods based on the state-space model and the frequency-domain methods based on the impedance model, phase-amplitude dynamics model [39]. In this section the time-domain analysis based on the state-space model has been considered.

TABLE 2. Initial steady-state values of generators and loads.

GENERATORS	MW	V_t
BUS 1	1350	1.0
BUS 4	3900	1.0
BUS 5	0.0	1.0
LOADS	**MW**	**MVar**
BUS 2	1250	0.0
BUS 3	4000	0.0

Fig. 15 shows the eigenvalue loci corresponding to the low-frequency oscillation of the two-area system for the three cases analyzed when X_L varies from 0.01 p.u. to 0.9 p.u. As can be seen in Fig. 15, the frequency of the mechanical oscillation modes (inter-area modes) decreases when the value of X_L increases (weak tie-line). If no damping is applied, the system can become unstable if the tie-line presents a value of X_L greater than 0.13 p.u. When a POD-Q control is applied using the PEC as a STATCOM, it is observed how the system damps the electromechanical oscillation modes for high values of X_L, although not as effectively as when a POD-P is used.

In this case, the PEC acts as a GFC and maintains a damping factor for the electromechanical modes at a value close to 20% regardless of the reactance of the line. This same effect is also observed for the flux-decay oscillation modes. Moreover, as can be seen, the POD-Q dampens the flux-decay oscillation modes less than when no PEC is connected.

In conclusion, POD-P is more effective than POD-Q in all the cases analyzed.

B. DYNAMIC RESPONSE TO A LOAD CHANGE

This section analyzes the dynamic response of the two-area system when a load reduction of 100 MW takes place in bus 2 at t = 0. The initial conditions are those indicated in Table 2. In this study, a value of $X_L = 0.1$ p.u (0.2 p.u in each line) has been considered which, as already mentioned, gives rise to stable operation, even without any compensation.

Fig. 16 shows the active and reactive power responses through the tie-line in the three cases analyzed. Power oscillations when the PEC is disabled (blue line) have a frequency

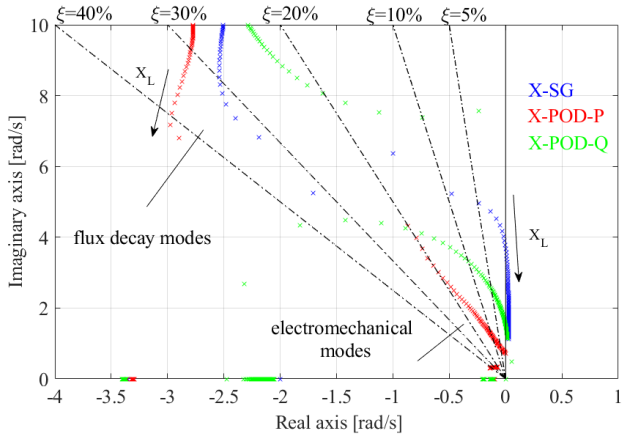

FIGURE 15. Eigenvalue loci of the two-area system under X_L variation for the three cases analyzed: a) SG b) POD-P (GFC) and c) POD-Q (STATCOM).

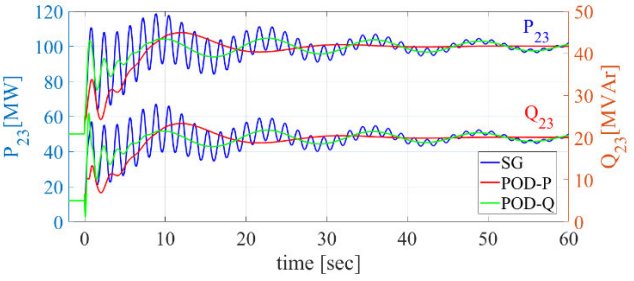

FIGURE 16. Active and reactive power transmitted by an interconnection line to a load change of 100 MW in bus 2 for the three cases analyzed: a) SG b) POD-P (GFC) and c) POD-Q (STATCOM).

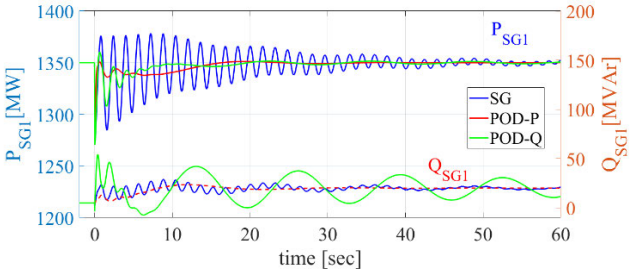

FIGURE 17. Active and reactive power response of SG1.

of 0.64 Hz and are weakly damped. Power damping increases when a POD-Q is applied, but is even greater with a POD-P, which reaches a damping factor of 20%. Initially, each tie-line transmits 50 MW of active power and 5 MVar of reactive power. After the load step, the power transmitted through the line increases to 100 MW and 20 MVar in steady state.

Figures 17 and 18 show the active and reactive power generated by synchronous areas SG1 and SG2, respectively. The power oscillations registered are the same as those indicated above. In the case of SG1, the active power remains constant in steady state after the load change (1350 MW) and the reactive power increases slightly. The reactive power presents low-frequency oscillation of 0.08 Hz and is poorly

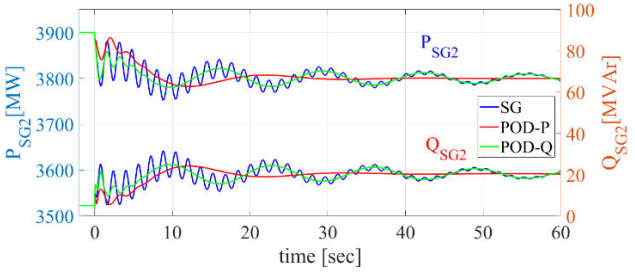

FIGURE 18. Active and reactive power response of SG2.

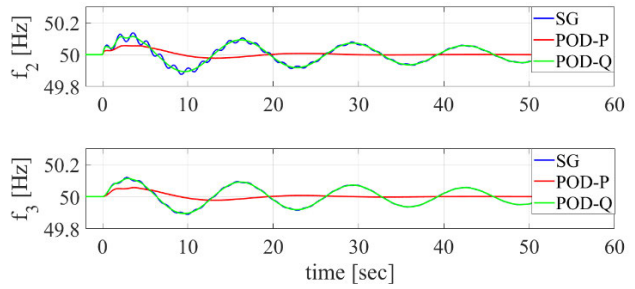

FIGURE 19. Frequency at bus 2 (f_2) and bus 3 (f_3).

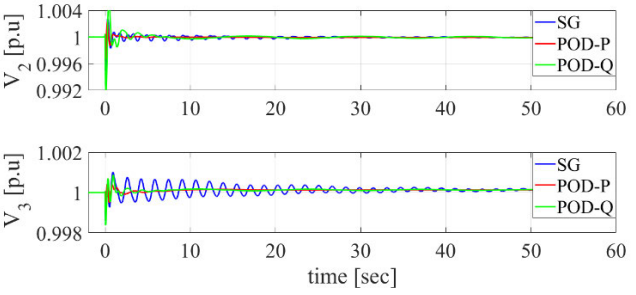

FIGURE 20. Voltages at bus 2 (V_2) and bus 3 (V_3).

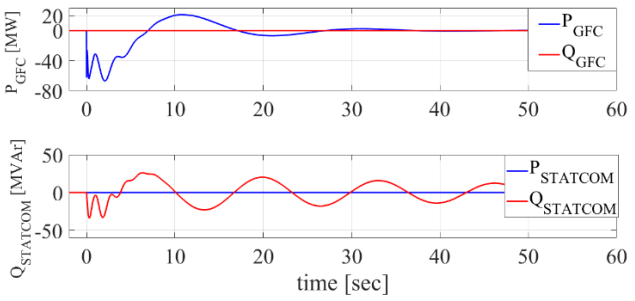

FIGURE 21. Active and reactive power exchange by the GFC(POD-P) and the STATCOM(POD-Q) during a load change event.

damped when a POD-Q is applied, which is consistent with the eigenvalues shown in Fig. 15.

However, in the case of SG2, the power is reduced by 100 MW (from 3900 MW to 3800 MW) in such a way that the load at node 3 (4000 MW) is covered with 200 MW from the lines and 3800 MW from synchronous area SG2.

Figure 19 shows the frequency variation at buses 2 (f_2 in top chart) and 3 (f_3 in bottom chart) in each of the cases studied.

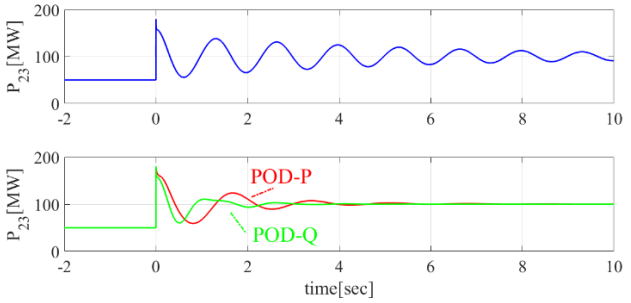

FIGURE 22. Active power transmitted by the interconnection tie during a line tripping event. With POD-P and POD-Q compensation (bottom figure) and without compensation (top figure).

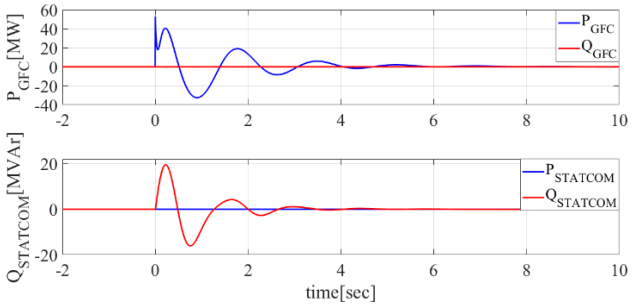

FIGURE 23. Active and reactive power exchange by the GFC(POD-P) and the STATCOM (POD-Q) during a line tripping event.

Active power oscillation in the tie-line is mainly caused by the angular voltage difference at the two ends of the line.

Likewise, Fig. 20 shows the voltages at buses 2 and 3. It is observed that the voltage variation is more significant at bus 2, especially when a POD-Q control strategy is used.

Finally, the active and reactive power exchanged by the PEC are presented in Fig. 21 in the case of POD-P (grid-forming converter) and POD-Q (STATCOM).

In the POD-P case, the GFC only exchanges active power, reactive power being zero. To damp the system, the converter absorbs a maximum power of 70 MW and injects a maximum power of 30 MW. When the frequency reaches steady state, the GFC stops exchanging active power. In the POD-Q case, it is just the opposite: the STATCOM exchanges only reactive power to damp the power oscillations, active power being zero. The reactive power exchange varies by ±25 MVar.

As has been shown throughout this paper, the POD-P strategy is more effective than the POD-Q strategy. However, this means that the converter requires some kind of energy supply connected to the DC terminals. In contrast, the STATCOM does not require energy supply, but its damping capability is much more limited. In any case, a GFC with storage does not require a battery with a high energy capacity. As shown in this example, compensation of the line required net energy absorption of approximately 40 kWh, which for a transmission line of these characteristics is not an excessively high value.

C. DYNAMIC RESPONSE TO A LINE TRIPPING

This section analyzes the dynamic response of the two-area system when one of the two lines connecting buses 2 and 3 (Fig. 14) is tripped. Initially each line transmits 50 MW and after the tripping (t = 0 s) the active power oscillates until reaching 100 MW in steady state, which is the power transmitted previously by the two interconnection lines. In the upper part of Fig. 22 the power oscillation through the healthy line, without any compensation, is shown. As it can be seen, this oscillation dampens in 10 s. At the bottom of Fig. 22 the power oscillation, when the line is compensated, with a GFC (POD-P) and with a STATCOM (POD-Q), are also shown. In both cases power oscillations are damped in less than 4 s, being the POD-Q slightly more effective.

Fig. 23 shows the active and reactive power exchanged for the GFC and the STATCOM during the line tripping event. As can be seen, the GFC (upper figure) uses around ±40 MW during the first oscillation to compensate the line oscillation and the STATCOM around ±20 MVar (bottom figure). Namely, in the case of line tripping the STATCOM is more effective since it exchanges less power and the damping of the line is slightly higher.

V. CONCLUSION

The increasing incorporation of renewable energies in power systems is causing growing concern about power system stability. Power electronic converters can contribute to system stability through the implementation of power system stabilizers. In this paper, two stabilizers have been proposed, demonstrating the ability of both stabilizers to damp low-frequency oscillations in power systems. The first stabilizer, named POD-P, has been implemented in a grid-forming converter and uses the GFC angle to damp system oscillations. Consequently, the GFC exchanges active power with the system while damping the oscillations. The second stabilizer, named POD-Q, has been implemented in a STATCOM and uses the STATCOM internal voltage magnitude to damp system oscillations. Accordingly, the STATCOM only exchanges reactive power with the system while damping the oscillations. Small-signal stability analysis has been carried out based on the linearized model of the system. This stability analysis has shown how the system eigenvalues become more stable after implementing the proposed PODs. Two cases have been considered —a single-machine system and a two-area system— in order to prove the ability of the proposed PODs to damp single-machine oscillations and inter-area oscillations. The effectiveness of the proposed PODs has also been proved through simulation, using comprehensive models of the nonlinear system. Simulation results, as well as the stability study, show the superiority of the POD-P stabilizer over the POD-Q, but at a cost of having to use some kind of energy supply in the DC bus to support the power interchange during system stabilization.

APPENDIX A
SYSTEM PARAMETERS AND OPERATION POINT

TABLE 3. System parameters.

PARAMETER	SYMBOL	VALUE	UNITS
Stator resistance	R_s	0.0	p.u.
d-axis synchronous reactance	X_d	1.8	p.u.
q-axis synchronous reactance	X_q	1.7	p.u.
d-axis transient reactance	X'_d	0.3	p.u.
Line resistance	R_e	0.0	p.u.
Line reactance	X_e	0.3	p.u.
d-axis transient open circuit constant	T'_{d0}	8.0	s
Inertia constant	H	6.175	s
Damping factor	D	0.0	p.u.
Exciter time constant	T_A	0.2	s
Exciter gain	K_A	200	p.u.
Frequency (50 Hz)	ω_s	314.16	rad/s
PEC reactance	X_g	0.15	p.u,
Washout time constant	T_w	1.00	s
Washout gain	K_w	3.00	p.u.
Droop gain	R_g	0.05	p.u.

TABLE 4. State variables and algebraic variables at the operation point when $V_\infty = 1$ p.u., $V_t = 1$ p.u., and $\theta = 9^0$.

STATE VARIABLES	SYMBOL	VALUE	UNITS
q-axis transient voltage	E'_q	0.8793	p.u.
q-axis angle	δ	48.647	degrees
Rotor speed	ω	314.159	rad/s
Excitation voltage	E_{fd}	1.4258	p.u.
ALGEBRAIC VARIABLES	**SYMBOL**	**VALUE**	**UNITS**
d-axis current	I_d	0.3643	p.u.
q-axis current	I_q	0.3753	p.u.
d-axis voltage	V_d	0.6381	p.u.
q-axis voltage	V_q	0.7700	p.u.
INPUTS	**SYMBOL**	**VALUE**	**UNITS**
Mechanical torque	T_m	0.5214	p.u.
Reference voltage	V_{ref}	1.0071	p.u.

APPENDIX B
LINEARIZED MODELS

The variable states of the single machine infinite-bus model (baseline case) are

$$\Delta x = [\Delta E'_q, \Delta\delta, \Delta\omega, \Delta E_{fd}]^t,$$

the vector of algebraic variables

$$\Delta y = [\Delta I_d, \Delta I_q, \Delta V_d, \Delta V_q]^t.$$

The input vector $\Delta u = [\Delta T_m, \Delta V_{ref}]^t$.

The nonzero values of the matrices A, B, C, D and E are as follows:

MATRIX A [4 × 4]

$$A_{11} = -\frac{1}{T'_{d0}} \quad A_{14} = +\frac{1}{T'_{d0}}$$
$$A_{23} = \omega_s$$
$$A_{31} = -\frac{I_q^0}{2H} \quad A_{33} = -\frac{D}{2H}$$
$$A_{44} = -\frac{1}{T_A}$$

MATRIX B [4 × 4]

$$B_{11} = -\frac{X_d - X'_d}{T'_{d0}}$$
$$B_{31} = -\frac{I_q^0}{2H}\left(X_q - X'_d\right)$$
$$B_{32} = -\frac{1}{2H}\left[E_q'^0 + (X_q - X'_d)I_d^0\right]$$
$$B_{43} = \frac{K_A}{T_A}\left(\frac{V_d^0}{V_t^0}\right) \quad B_{44} = \frac{K_A}{T_A}\left(\frac{V_q^0}{V_t^0}\right)$$

MATRIX C [4 × 4]

$$C_{21} = 1$$
$$C_{32} = -V_\infty cos\delta^0$$
$$C_{42} = +V_\infty sin\delta^0$$

MATRIX D [4 × 4]

$$D_{12} = X_q \quad D_{13} = -1$$
$$D_{21} = -X'_d \quad D_{24} = -1$$
$$D_{32} = X_e \quad D_{33} = +1$$
$$D_{41} = -X_e \quad D_{44} = +1$$

MATRIX E [4 × 2]

$$E_{31} = \frac{1}{2H}$$
$$E_{42} = \frac{K_A}{T_A}$$

Matrices A, B, C and D of the model of a SG and a grid-forming converter connected to an infinite bus are given below. In this model, the vector of variable states is extended with two additional states, $\Delta\delta_g$ and Δz. The nonzero elements of matrices A and B are the same as those indicated in the base case (single-machine infinite-bus) plus the following:

MATRIX A [6 × 6]

$$A_{52} = -R_g K_s \omega_s \quad A_{53} = -K_w \omega_s \quad A_{56} = +K_w \omega_s$$
$$A_{63} = \frac{1}{T_w} \quad A_{66} = -\frac{1}{T_w}$$

MATRIX B [6 × 4]

$$B_{53} = \left(\frac{E_g^0}{X_g K_s}\right)\left[\left(\frac{V_d^0}{V_t^0}\right) sin\left(\delta^0 - \theta^0\right) - 1\right]$$
$$B_{54} = \left(\frac{E_g^0}{X_g K_s}\right)\left[\left(\frac{V_q^0}{V_t^0}\right) sin\left(\delta^0 - \theta^0\right)\right]$$

MATRIX C [4 × 6]

$$C_{21} = 1$$
$$C_{32} = -\left(K_g E_g^0 \cos\left(\delta_g^0 - \delta^0\right) + K_e V_\infty cos\delta^0\right)$$
$$C_{35} = K_g E_g^0 \cos\left(\delta_g^0 - \delta^0\right)$$
$$C_{41} = -K'_d$$
$$C_{42} = -\left(K_g E_g^0 \sin\left(\delta_g^0 - \delta^0\right) - K_e V_\infty sin\delta^0\right)$$
$$C_{45} = K_g E_g^0 \sin\left(\delta_g^0 - \delta^0\right)$$

MATRIX D [4 × 4]

$$D_{12} = X_q \quad D_{13} = -1$$
$$D_{21} = -X'_d \quad D_{24} = -1$$
$$D_{32} = -K'_d \left(X_q - X'_d\right) \quad D_{33} = +1$$
$$D_{44} = +1$$

MATRIX E [6 × 2]

The nonzero elements of matrix E are the same as in the baseline case. Now, the order of matrix E is 6 × 2.

Matrices A, B, C and D of the model of a SG and a STATCOM connected to an infinite bus are given below. In this model, the vector of variable states is extended with one additional state, Δz. The nonzero elements of matrix A are the same as those indicated in the baseline case (single-machine infinite-bus) plus the following:

MATRIX A [5 × 5]

$$A_{53} = \frac{1}{T_w} \quad A_{55} = -\frac{1}{T_w}$$

MATRIX B [5 × 4]

The nonzero elements of matrix B are the same as in the baseline case.

MATRIX C [4 × 5]

$$C_{21} = 1$$
$$C_{32} = -\left(K_g E_g^0 \cos\left(\theta^0 - \delta^0\right) + K_e V_\infty cos\delta^0\right)$$
$$C_{33} = K_g K_w \sin\left(\theta^0 - \delta^0\right)$$
$$C_{35} = -K_g K_w \sin\left(\theta^0 - \delta^0\right)$$
$$C_{41} = -K'_d$$
$$C_{42} = -\left(K_g E_g^0 \sin\left(\delta_g^0 - \delta^0\right) - K_e V_\infty sin\delta^0\right)$$
$$C_{43} = -K_g E_g^0 \cos\left(\delta_g^0 - \delta^0\right)$$
$$C_{45} = +K_g E_g^0 \cos\left(\delta_g^0 - \delta^0\right)$$

MATRIX D [4 × 4]

The nonzero elements of matrix D are the same as in the baseline case

MATRIX E [5 × 2]

The nonzero elements of matrix E are the same as in the baseline case. Now, the order of matrix E is 5 × 2.

APPENDIX C

TABLE 5. GENROU parameters.

H=6,3s ,D=0, $Td0'$=6,47, $Td0''$=0,022, $Tq0'$=0,61, $Tq0''$=0,034 xd=2,135 , xq=2,046 , xd'=0,34 , xq'=0,573, xd''=xq''=0,269, xl=0,234 $s1$=0,1275 , $s2$=0,2706

TABLE 6. Excitation system model IEEE type ST1.

T_R=0,01s, T_B=10s, T_c=1s, K_A=200, T_A=0s Vi_{max}=999 , Vi_{min}=−999 , $V_{R,max}$=999 , $V_{R,min}$=−999 , K_c=K_F=0, T_F=1s

TABLE 7. Speed governor model and turbine IEEEG1.

K=20, K_1=0,3, K_3=0,3 , K_5=0,4 , K_7=0 T_1=T_2=0, T_3=0,1s , T_4=0,3s , T_5=7s , T_6=0,6s , T_7=0 K_2=K_4= K_6=K_8=0, U_0=0.5 , U_c=−0.5 , P_{max}=1, P_{min}=0

REFERENCES

[1] N. Hatziargyriou, J. Milanovic, C. Rahmann, V. Ajjarapu, C. Cañizares, I. Erlich, D. Hill, I. Hiskens, I. Kamwa, B. Pal, and P. Pourbeik, "Stability definitions and characterization of dynamic behavior in systems with high penetration of power electronic interfaced technologies," IEEE Power Energy Soc., Piscataway, NJ, USA, Tech. Rep. PES-TR77, 2020.

[2] P. Kundur, J. Paserba, V. Ajjarapu, G. Andersson, A. Bose, C. Canizares, N. Hatziargyriou, D. Hill, A. Stankovic, C. Taylor, T. Van Cutsem, and V. Vittal, "Definition and classification of power system stability IEEE/CIGRE joint task force on stability terms," *IEEE Trans. Power Syst.*, vol. 19, no. 3, pp. 1387–1401, Aug. 2004.

[3] P. Tielens and D. Van Hertem, "The relevance of inertia in power systems," *Renew. Sustain. Energy Rev.*, vol. 55, pp. 999–1009, Mar. 2016.

[4] D. Gautam and V. Vittal, "Impact of DFIG based wind turbine generators on transient and small signal stability of power systems," in *Proc. IEEE Power Energy Soc. Gen. Meeting*, Jul. 2009, pp. 1–6.

[5] G. Tsourakis, B. M. Nomikos, and C. D. Vournas, "Effect of wind parks with doubly fed asynchronous generators on small-signal stability," *Electr. Power Syst. Res.*, vol. 79, no. 1, pp. 190–200, Jan. 2009.

[6] S. Eftekharnejad, V. Vittal, G. T. Heydt, B. Keel, and J. Loehr, "Small signal stability assessment of power systems with increased penetration of photovoltaic generation: A case study," *IEEE Trans. Sustain. Energy*, vol. 4, no. 4, pp. 960–967, Oct. 2013.

[7] P. Kundur, *Power System Stability and Control*. Palo Alto, CA, USA: McGraw-Hill, 2007.

[8] *IEEE Recommended Practice for Excitation System Models for Power System Stability Studies*, IEEE Standard 421.5-2016 (Revision IEEE Standard 421.5-2005), Aug. 2016, pp. 1–207.

[9] F. Rashidi and M. Rashidi, "Robust and adaptive tuning of power system stabilizers using artificial neural networks," in *Proc. Int. Conf. Ind., Eng. Other Appl. Appl. Intell. Syst.* Berlin, Germany: Springer, May 2004, pp. 1023–1032.

[10] N. P. Patidar, M. L. Kolhe, N. P. Tripathy, B. Sahu, A. Sharma, L. K. Nagar, and A. N. Azmi, "Optimized design of wide-area PSS for damping of inter-area oscillations," in *Proc. IEEE 11th Int. Conf. Power Electron. Drive Syst.*, Jun. 2015, pp. 1172–1177.

[11] N. G. Hingorani and L. Gyugyi, *Understanding FACTS: Concepts and Technology of Flexible AC Transmission Systems*. New York, NY, USA: IEEE, 2000.

[12] M. Beza and M. Bongiorno, "An adaptive power oscillation damping controller by STATCOM with energy storage," *IEEE Trans. Power Syst.*, vol. 30, no. 1, pp. 484–493, Jan. 2015.

[13] S. Feng, X. Wu, P. Jiang, L. Xie, and J. Lei, "Mitigation of power system forced oscillations: An E-STATCOM approach," *IEEE Access*, vol. 6, pp. 31599–31608, 2018.

[14] L. Zeni, R. Eriksson, S. Goumalatsos, M. Altin, P. Sørensen, A. Hansen, P. Kjær, and B. Hesselbæk, "Power oscillation damping from VSC–HVDC connected offshore wind power plants," *IEEE Trans. Power Del.*, vol. 31, no. 2, pp. 829–838, Apr. 2016.

[15] J. Björk, K. H. Johansson, and L. Harnefors, "Fundamental performance limitations in utilizing HVDC to damp interarea modes," *IEEE Trans. Power Syst.*, vol. 34, no. 2, pp. 1095–1104, Mar. 2019.

[16] X. Sui, Y. Tang, H. He, and J. Wen, "Energy-storage-based low-frequency oscillation damping control using particle swarm optimization and heuristic dynamic programming," *IEEE Trans. Power Syst.*, vol. 29, no. 5, pp. 2539–2548, Sep. 2014.

[17] K. M. Alawasa, Y. A.-R.-I. Mohamed, and W. Xu, "Modeling, analysis, and suppression of the impact of full-scale wind-power converters on subsynchronous damping," *IEEE Syst. J.*, vol. 7, no. 4, pp. 700–712, Dec. 2013.
[18] M. Basu, V. R. Mahindara, J. Kim, R. M. Nelms, and E. Muljadi, "Comparison of active and reactive power oscillation damping with PV plants," *IEEE Trans. Ind. Appl.*, vol. 57, no. 3, pp. 2178–2186, May 2021.
[19] W. Zhang, A. Tarraso, J. Rocabert, A. Luna, J. I. Candela, and P. Rodriguez, "Frequency support properties of the synchronous power control for grid-connected converters," *IEEE Trans. Ind. Appl.*, vol. 55, no. 5, pp. 5178–5189, Sep. 2019.
[20] J. Rocabert, A. Luna, F. Blaabjerg, and P. Rodriguez, "Control of power converters in AC microgrids," *IEEE Trans. Power Electron.*, vol. 27, no. 11, pp. 4734–4749, Nov. 2012.
[21] S. Yazdani, M. Ferdowsi, M. Davari, and P. Shamsi, "Advanced current-limiting and power-sharing control in a PV-based grid-forming inverter under unbalanced grid conditions," *IEEE J. Emerg. Sel. Topics Power Electron.*, vol. 8, no. 2, pp. 1084–1096, Jun. 2020.
[22] S. D'Arco and J. A. Suul, "Equivalence of virtual synchronous machines and frequency-droops for converter-based microgrids," *IEEE Trans. Smart Grid*, vol. 5, no. 1, pp. 394–395, Jan. 2014.
[23] Q.-C. Zhong, P.-L. Nguyen, Z. Ma, and W. Sheng, "Self-synchronized synchronverters: Inverters without a dedicated synchronization unit," *IEEE Trans. Power Electron.*, vol. 29, no. 2, pp. 617–630, Feb. 2014.
[24] P. Rodriguez, C. Citro, J. I. Candela, J. Rocabert, and A. Luna, "Flexible grid connection and islanding of SPC-based PV power converters," *IEEE Trans. Ind. Appl.*, vol. 54, no. 3, pp. 2690–2702, May 2018.
[25] X. Meng, J. Liu, and Z. Liu, "A generalized droop control for grid-supporting inverter based on comparison between traditional droop control and virtual synchronous generator control," *IEEE Trans. Power Electron.*, vol. 34, no. 6, pp. 5416–5438, Jun. 2019.
[26] G. N. Baltas, N. B. Lai, L. Marin, A. Tarraso, and P. Rodriguez, "Grid-forming power converters tuned through artificial intelligence to damp subsynchronous interactions in electrical grids," *IEEE Access*, vol. 8, pp. 93369–93379, 2020.
[27] A. P. Asensio, S. A. Gomez, J. L. Rodriguez-Amenedo, and M. A. Cardiel-Alvarez, "Reactive power synchronization method for voltage-sourced converters," *IEEE Trans. Sustain. Energy*, vol. 10, no. 3, pp. 1430–1438, Jul. 2019.
[28] J. L. R. Amenedo, S. A. Gómez, J. Alonso-Martinez, and M. G. De Armas, "Grid-forming converters control based on the reactive power synchronization method for renewable power plants," *IEEE Access*, vol. 9, pp. 67989–68007, 2021.
[29] L. Huang, H. Xin, and Z. Wang, "Damping low-frequency oscillations through VSC-HVDC stations operated as virtual synchronous machines," *IEEE Trans. Power Electron.*, vol. 34, no. 6, pp. 5803–5818, Jun. 2019.
[30] *Technical Regulation Normative and Supervision Conformity of Electricity Generator Modules According to EU Regulation 2016/631*, Red Eléctr. de España, Alcobendas, Spain, 2021.
[31] F. P. Demello and C. Concordia, "Concepts of synchronous machine stability as affected by excitation control," *IEEE Trans. Power App. Syst.*, vol. PAS-88, no. 4, pp. 316–329, Apr. 1969.
[32] W. G. Heffron and R. A. Phillips, "Effect of a modern amplidyne voltage regulator on underexcited operation of large turbine generators [includes discussion]," *Trans. Amer. Inst. Electr. Eng. III, Power App. Syst.*, vol. 71, no. 3, pp. 692–697, Aug. 1952.
[33] P. W. Sauer and M. A. Pai, *Power System Dynamics and Stability*, vol. 101. Upper Saddle River, NJ, USA: Prentice-Hall, 1998.
[34] X. Xiong, C. Wu, P. Cheng, and F. Blaabjerg, "An optimal damping design of virtual synchronous generators for transient stability enhancement," *IEEE Trans. Power Electron.*, vol. 36, no. 10, pp. 11026–11030, Oct. 2021.
[35] C. A. Cañizares, M. Pozzi, S. Corsi, and E. Uzunovic, "STATCOM modeling for voltage and angle stability studies," *Int. J. Electr. Power Energy Syst.*, vol. 25, no. 6, pp. 431–441, Jul. 2003.
[36] P. Pourbeik, B. Agrawal, S. Patterson, and R. Rhinier, "Modeling of synchronous generators in power system studies," *Cigre Sci. Eng.*, vol. 6, pp. 21–32, Oct. 2016.
[37] R. Zárate-Miñano, F. Milano, and A. J. Conejo, "An OPF methodology to ensure small-signal stability," *IEEE Trans. Power Syst.*, vol. 26, no. 3, pp. 1050–1061, Aug. 2011.
[38] T. J. M. A. Parreiras, S. Gomes, Jr., G. N. Taranto, and K. Uhlen, "Closest security boundary for improving oscillation damping through generation redispatch using eigenvalue sensitivities," *Electr. Power Syst. Res.*, vol. 160, pp. 119–127, Jul. 2018.
[39] L. Xiong, X. Liu, Y. Liu, and F. Zhuo, "Modeling and stability issues of voltage-source converter dominated power systems: A review," *CSEE J. Power Energy Syst.*, early access, Nov. 20, 2020, doi: 10.17775/CSEEJPES.2020.03590.

JOSÉ LUIS RODRÍGUEZ-AMENEDO (Senior Member, IEEE) received the M.S. degree in industrial engineering from the University Polytechnic of Madrid, in 1994, and the Dr.-Ing. (Ph.D.) degree in industrial engineering from the University Carlos III of Madrid, in 2000. From 1999 to 2000, he was with Iberdrola Engineering as a Technology Wind Turbine Manager. From 2001 to 2003, he was with Iberdrola Renewables as a Wind Energy Manager. In 2003, he joined the Electrical Department, University Carlos III, as an Associate Professor. From 2008 to 2011, he requested an academic leave of absence for founding the technological companies Energy to Quality (E2Q) and Wind to Power Systems (W2PS). His research interests include renewable energy integration into the grid, power electronic converter control, HVDC transmission systems, and energy storage solutions.

SANTIAGO ARNALTES GÓMEZ received the Ph.D. degree in industrial engineering from the Polytechnical University of Madrid, in 1993. He is currently a Full Professor in electrical engineering at the Carlos III University of Madrid. His research interests include modeling, simulation, and control of renewable energy systems, and energy storage systems.